Book Chapter

Graphene-Based Electrodes for Silicon Heterojunction Solar Cell Technology

Susana Fernández[1]*, Ignacio Torres[1]*, Julio Cárabe[1], Israel Arnedo[2,3] and José Javier Gandía[1]

[1]Departamento de Energías Renovables, Centro de Investigaciones Energéticas, Medioambientales y Tecnológicas (CIEMAT), Spain
[2]Das-Nano, Polígono Industrial Talluntxe, Spain
[3]Departamento Ingeniería Eléctrica, Electrónica y de Comunicación, Universidad Pública de Navarra, Spain

***Corresponding Authors:** Susana Fernández, Departamento de Energías Renovables, Centro de Investigaciones Energéticas, Medioambientales y Tecnológicas (CIEMAT), Madrid 28040, Spain

Ignacio Torres, Departamento de Energías Renovables, Centro de Investigaciones Energéticas, Medioambientales y Tecnológicas (CIEMAT), Madrid 28040, Spain

Published **December 29, 2021**

This Book Chapter is an excerpt from articles published by Susana Fernández, et al. and I Torres, et al. at Micromachines and Materials respectively. (Fernández, S.; Molinero, A.; Sanz, D.; González, J.P.; Cruz, M.d.l.; Gandía, J.J.; Cárabe, J. Graphene-Based Contacts for Optoelectronic Devices. Micromachines 2020, 11, 919. https://doi.org/10.3390/mi11100919) (Torres, I.; Fernández, S.; Fernández-Vallejo, M.; Arnedo, I.; Gandía, J.J. Graphene-Based Electrodes for Silicon Heterojunction Solar Cell Technology. Materials 2021, 14, 4833. https://doi.org/10.3390/ma14174833)

How to cite this book chapter: Susana Fernández, Ignacio Torres, Julio Cárabe, Israel Arnedo, José Javier Gandía.

Graphene-Based Electrodes for Silicon Heterojunction Solar Cell Technology. In: M Iqbal Khan, editor. Prime Archives in Material Science: 3rd Edition. Hyderabad, India: Vide Leaf. 2021.

Conflicts of Interest: The authors declare no conflict of interest.

Author Contributions: Conceptualization, I.T., J.C., J.J.G. and S.F.; methodology, I.T, S.F. and I.A.; validation, S.F., I.T. and I.A.; formal analysis, I.T., S.F. and I.A.; investigation, I.T., S.F. and I.A.; resources, J.C., J.J.G. and I.A.; writing—original draft preparation, I.T. and S.F.; writing—review and editing, J.C., I.T. and S.F.; project administration, J.C. and J.J.G.; funding acquisition, J.J.G. and J.C.. All authors have read and agreed to the published version of the manuscript.

Funding: This research was funded by grant ENE2017-88065-C2-2-R (DIGRAFEN), and grant PID2020-114234RB-C21 (REGRAP-2D) funded by MCIN/AEI/ 10.13039/501100011033. Das-Nano and UPNA would also like to acknowledge the funding from the Government of Navarra and the European Regional Development Fund (ERDF), 2020 I+D projects: ref. 0011-1365-2020-000026 for das-Nano and ref. 0011-1365-2020-000045 for UPNA.

Acknowledgments: The authors would like to acknowledge David Canteli and the Centro Láser of the Universidad Politécnica de Madrid for the Raman characterization of the samples, to A. Molinero, D. Sanz, J.P. Gonzalez and M. de la Cruz from CIEMAT for their technical support. The authors would like to acknowledge das-Nano Terahertz Business Unit for providing conductance maps of the samples using ONYX system.

Abstract

Transparent conductive electrodes (TCEs) based on graphene have been previously proposed as an attractive candidate for optoelectronic devices. While graphene alone lacks the antireflectance properties needed in many applications, it can still be coupled with traditional transparent conductive oxides (TCOs), further enhancing their electrical performance.

In this work, new architectures of TCEs incorporating graphene monolayers in different spatial configurations have been explored. The aim is to achieve advanced transparent electrodes specifically designed to minimize surface reflection over a wide range of wavelengths and angles of incidence and to improve electrical performance. Furthermore, these hybrid electrodes are designed to improve the performance of silicon heterojunction (SHJ) solar cell front transparent contacts. These structures consist of combinations of a conventional TCO with a few graphene monolayers. The most suitable strategies for their fabrication have been assessed by testing different approaches that addresses issues such as the protection of the device structure underneath, the limitation of sample temperature during the graphene-monolayer transfer process and the determination of the most suitable stacking structure. The results reveal a strong dependence of the optoelectronic properties of the TCEs on (i) the spatial configuration of the different layers involved and and (ii) the specific TCO material used. The best results were obtained when ITO was used as the TCO and the graphene layers were transferred on top of the TCO.

Finally, the effect of combining indium tin oxide (ITO) with between 1 and 3 graphene monolayers as the top electrode in the SHJ technology has been analysed. Each additional graphene monolayer is shown to improve the sheet resistance of the hybrid electrode. In the electrical characterization of the finished solar cells, this translates into a meaningful reduction of the series resistance and into an increase of the device' fill factor. On the other hand, each additional sheet absorbs part of the incoming radiation, causing the short circuit current to simultaneously decrease. Consequently, additional graphene monolayers past the

first one did not further enhance the efficiency of the reference cells. Ultimately, the increase obtained in the fill factor endorse graphene-based hybrid electrodes as a potential concept for improving solar cells' efficiency in future novel designs.

Introduction

Although graphite, one of the crystallographic forms of carbon, has been relatively well known for a long time, its two-dimensional version—graphene—is a much more recent object of research. The lamellar structures of graphite and of thermally reduced graphite oxide were already known in the mid-19th century [1], but it still took about ninety years until the first theoretical studies on single atomic graphite layers were undertaken and the first electron-microscopy images of a few-layer graphite sample were published [2]. Despite these partial milestones, the inception of graphene technology had to wait another half century before André Geim and Kostya Novoselov at the University of Manchester were able to obtain single-atom layers from a graphite sample in 2004 [3]. The method was based on peeling single graphite layers and transferring them onto a monocrystalline-silicon wafer coated with silicon dioxide by following a procedure called micromechanical cleavage.

Graphene is a material made of a single layer of carbon atoms distributed in the vertexes of a hexagonal network. This hexagonal shape (honeycomb) results from the covalent bonds generated by the overlap of the sp^2 hybrid orbitals of the mutually-bonded carbon atoms. It is therefore a two-dimensional material (2D). Such an atomic arrangement and its two-dimensional structure are the factors conferring extraordinary properties to graphene. Graphene is a zero-gap semiconductor. Its electron mobility is extremely high, of the order of 150,000–200,000 $cm^2V^{-1}s^{-1}$. Optically, a single layer of graphene absorbs 2.3% of incident light, allowing around 97.7% to pass through [4]. Thus, as a rule of thumb, when working with graphene multilayers, one can estimate a 2.3% transmittance loss per atomic layer. The degree of reflection from single-layer graphene is almost negligible, just less than 0.1%, rising to no more than 2% for ten atomic layers [5]. Finally, graphene is not a self-

standing material. Once deposited, it must be transferred onto a substrate conferring to it the necessary mechanical stability among other conditions. But the sensitivity of graphene and of its charge-conduction mechanisms to the interaction with the substrate or any other adjacent substance is not at all negligible. Therefore, the choice of the material to be combined with graphene needs careful consideration from a mechanical and electrical point of view.

Many of the described properties of this new material are outstanding in many senses, but for the purpose of the present work, the above-mentioned electrical and optical features are particularly relevant. Graphene offers excellent sheet conductance in combination with a very low absorption of light (for one or a few atomic layers), added to an extremely low reflection to visible light, all of this without adding more than a few angstrom to the final thickness. Thus, graphene is an excellent candidate to be used in those optoelectronic applications in which low sheet resistances, exceptional responses at high frequencies, low contact resistances or reduced light absorption are required. A wide range of optoelectronic devices such as light emitting diodes, photodiodes, liquid-crystal displays, touch screens or solar cells require transparent or semi-transparent contacts having such properties [6]. In addition, many of these optoelectronic devices typically use transparent conductive oxides (TCOs), such as fluorine doped tin oxide (SnO_2:F) abbreviated as FTO, indium tin oxide (In_2O_3:SnO_2) abbreviated as ITO, and aluminium doped zinc oxide (ZnO:Al_2O_3), abbreviated as AZO. They usually play the role as transparent electrodes, and thus, they must have n-type conductivity [7]. The TCOs are fabricated by using a wide variety of methods such as chemical vapour deposition (CVD), magnetron sputtering, sol–gel process or spray pyrolysis [8]. Among them, although magnetron sputtering can be considered too expensive for some industrial applications, it has two special advantages: (i) its great scalability to large areas, and (ii) its easiness to achieve thin films with good performance even if fabricated outside its thermodynamic equilibrium. Both characteristics are relatively important to make a success of the incorporation of the thin films into the low-temperature device

technology [9]. For these reasons, in the present work, magnetron sputtering is chosen to fabricate the TCO materials.

Among the different TCO materials, ITO is currently the most commonly used in optoelectronic devices. This semiconductor material is well-known from its mass production and exhibits suitable optoelectronic properties. Generally, ITO is deposited by direct current (DC) magnetron sputtering on large areas [10]. Otherwise, AZO is also used in several technologies. AZO is one of the very few alternative candidates for the replacement of indium based TCOs. This is due to its low-cost, its abundance, and its chemical stability in hydrogen plasma, in comparison with other TCOs [11]. Optically, these two well-known materials achieve a reasonable transmittance in the visible region of the electromagnetic spectrum of >80% [12]. But in certain applications requiring limited TCO thicknesses such as in solar cells front contacts, the sheet resistance is usually in the range 100-120 Ω/sq [13]. Front contacts play an important role in solar cells to achieve both efficient carrier collection and transport properties. Furthermore, contact resistances and optical reflectances would contribute to better device performances if they were improved (i.e. reduced). In this sense, hybrid concepts combining various kinds of nanoscale materials have been attempted. For example, the incorporation of carbon nanotubes (CNT) [14], metal nanowires/nanogrids [15,16], graphene or reduced graphene oxide (rGO) [17,18] have already been demonstrated, showing successful results. Among them, sheet resistances of 24 Ω/sq and 83% of average transmittance have been reported by CNT-based electrodes [14]. In the case of graphene fabricated by chemical vapour deposition (CVD), a wide range of values are found depending on the transfer techniques [19]. It is worth noting that in all these cases, the graphene replaces the TCO commonly used.

In the field of solar cells, silicon heterojunction (SHJ) solar cells are securing a space in the large-volume manufacturing PV market, currently dominated by back-surface-field (BSF) cells, and the Passivated Emitter Rear Cell (PERC) and passivated emitter rear totally diffused (PERT) cells, thanks to its impressive efficiencies and relatively simple structure [20]. In

SHJ solar cells, the front TCO contact needs high transparency and high electrical conductivity, qualities associated with graphene as well as with many other nano scale materials. However, in the case of SHJ solar cells, the TCO also serves as an antireflectance (AR) coating. Therefore, any substitute of the TCO in SHJ technology needs to address this, otherwise the solar cell efficiency can be highly hindered [23].

One way to benefit from nanomaterials exciting properties while providing with AR characteristics is by fabricating hybrid electrodes. For example, hybrid structures based on ITO and graphene have already shown excellent electrical and optical properties [24, 25] suitable to be implemented in SHJ solar cells. With this premise in mind, in this chapter the concept of transparent hybrid electrodes based on the most commonly TCOs used in SHJ technology, namely ITO and AZO, and graphene monolayers (GML) grown via CVD is explored further. The main reason for this choice is to avoid deviating too much from the materials used in the industry [10].

The purpose of this research is therefore finding a suitable combination of graphene and any of the selected TCOs to be applied as a transparent electrode in SHJ solar cells as well as other optoelectronic devices. The evaluation of preparation conditions compatible with the integrity of the properties of both materials has been treated as a key issue. In addition, hybrid electrodes with up to 3 GML are tested. The hybrid electrodes are fabricated directly in SHJ structures before metal grid deposition. The results obtained from the characterization of the hybrid electrodes and the properties of the finished solar cells are closely related. The quality of the graphene layers was established through Raman measurements, whereas the AR properties of the hybrid electrodes was evaluated through reflectance spectroscopy. Contactless measurements of the electrodes sheet resistance were realized through THz time domain spectroscopy, illustrating how the hybrid electrodes exhibit a lower sheet resistance with increasing the number of GML. Thanks to the lower sheet resistance, the finished solar cells with hybrid electrodes showed improvements in the series resistance and FF when compared with the reference cell with

only ITO. On the other hand, by increasing the number of GML, the transmittance of the hybrid electrodes decreased accordingly and J_{sc} was negatively affected. However, by limiting the number of GML to only one, the gains in FF outmatched the losses in J_{sc} and the efficiency of the devices improve with respect the reference cell. These results highlight the potential for the development of advanced transparent or semi-transparent electrodes based on graphene and its application to optoelectronic devices.

Materials and Methods

Graphene-based Transparent Electrode Fabrication

The hybrid transparent contacts described are based on the combination of a common TCO and 1 to 3 GML.

The GML were grown by Spanish company Graphenea S.L. by chemical vapour deposition (CVD) on copper foil from CH_4 precursor, prepped for transfer with polymethylmethacrylate (PMMA) coating, and finally transferred to the desired substrate. The CVD fabrication technique was preferred because it can produce relatively high-quality and high-purity graphene and potentially on a large scale. More details about the graphene fabrication can be found in reference [14].

The TCO materials were fabricated using a commercial Leybold UNIVEX 450B magnetron sputtering system (Leybold GmbH, Cologne, Germany). AZO was deposited by using a ceramic 4-inch $ZnO:Al_2O_3$ (98/2wt.%, Neyco, Vanves, France) commercial target subject to radio-frequency (RF), and ITO was obtained from a ceramic 4-inch $In_2O_3:SnO_2$ (90/10 wt.%, Neyco) commercial target subject to DC. Argon of a purity of 99.999% was used as the inert gas in the sputtering process, and the control of its flux was carried out by means of a mass-flow controller. TCO films were deposited at low temperature to work in conditions compatible with the preparation of different kinds of optoelectronic devices having a particular sensitivity to high temperatures.

Different combinations of TCO and graphene were tested, with different deposition and transfer sequences in order to assess technological paths taking into account the mutual compatibility of the processes involved as well as the properties of the resulting multilayers. In Figure 1a) the GML were transferred onto a TCO-coated substrate. In Figure 1b), the TCO layer was sputtered on top of the GML previously transferred onto the substrate.

For the electrical and transmittance measurements, the substrate used was either a high resistance glass or a quartz substrate. The substrates were ultrasonically cleaned using DECON 90 detergent, rinsed in deionized water, and immersed for 2 minutes in isopropyl alcohol before drying under a stream of nitrogen. For the reflectance measurements, the TCE structure were deposited on 4-inch polished resistive float zone <100> silicon wafers (resistivity > 10^4 Ω-cm). The native silicon oxide (SiO_x) was removed from the silicon-wafer surface by chemical etching in a dilute (2%) hydrofluoric acid prior to the TCE fabrication. After that, the wafer was rinsed in deionized water and dried under a stream of nitrogen.

Figure 1: TCE configurations under study (a) configuration 1, and (b) configuration 2.

In the particular case of the configuration 1, an Ar plasma bias etching on the substrate surface was carried out at 120 W under 0.5 Pa for 5 minutes without intentional heating prior to the sputtering deposition. This process was used to improve TCO thin-film adherence. After that, the substrate was rotated at 20 rpm, and heated at 190 °C in the holder system. Regardless of the TCO material deposited, the gas flow rate and the working pressure were maintained constant at 5 sccm and 0.18 Pa,

respectively. The samples were sputtered at the constant values of 75 W– DC power and 250 W–RF power applied to ITO and AZO targets, respectively. In the case of configuration 2, no bias was applied and softer sputtering conditions were used to avoid the possible damage to GML structure, that is, at room temperature and 25 W– DC power and 150 W– RF applied to ITO and AZO targets, respectively.

Silicon Heterojunction Solar Cells Fabrication

SHJ solar cells were fabricated using 280 µm thick flat n-type float zone c-Si <100> with a resistivity of 1-5 Ω·cm. After RCA cleaning, the wafers were stripped of the native oxide by dipping the substrates 1 minute in a 2% HF solution. The wafers were then loaded in a two-chamber PECVD reactor (Elettrorava s.p.a.) where ~5 nm thick intrinsic a-Si:H layers were deposited on both sides to ensure a good surface passivation. The back side of the wafer was then covered with a ~20 nm n-type a-Si:H film to form the back surface field and electron-selective contact whereas the front hole-selective contact was realized with the deposition of ~10 nm p-type a-Si:H layer. Following, an 80 nm thick ITO layer was sputtered on the front side through 3.5 cm^2 shadow masks. At this point, the GML were transferred onto the ITO surface. For the current research, we chose to test the effect of adding between 1 and 3 monolayers. Finally, after graphene deposition, Ti and Ag metal contacts were evaporated on the front (through a grid) and on the back (full area) and the cells were annealed 5 minutes at 200ºC in a hot plate to recover the passivation lost during the ITO sputtering process [26]. A sketch of the finished solar cells is depicted in Figure 2.

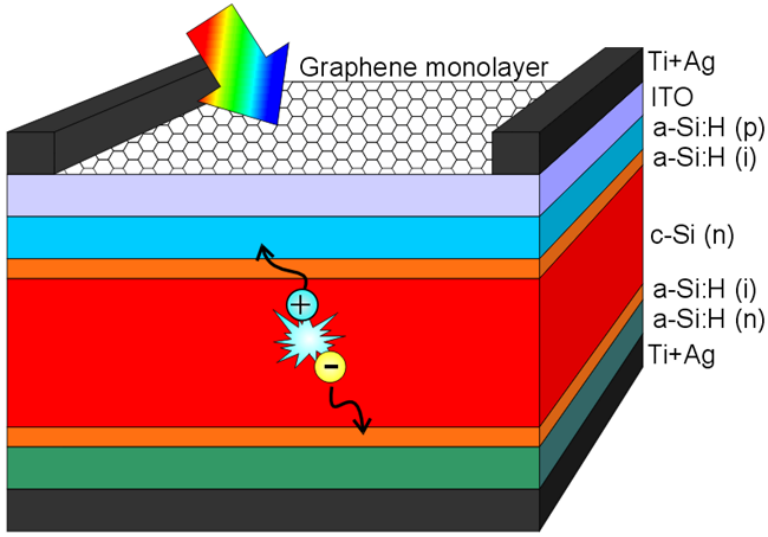

Figure 2: Sketch of the finished silicon heterojunction solar cell, in which the front ITO layer has been replaced with a graphene-based hybrid transparent conductive electrode consisting in a 80 nm thick ITO layer and a stack of up to three graphene monolayers.

Characterization Techniques

To characterize the GML, several characterization techniques were applied. Raman microscopy using a 514 nm Ar laser (inVia Renishaw) was used to check the quality of the films and to corroborate the number of graphene films transferred [27].

Total optical reflectance spectra were carried out in a UV/Visible/NIR Lambda 1050 Perkin Elmer spectrophotometer in the wavelength range from 300 to 1500 nm by using a 6 mm integrating sphere accessory. From these measurements the weighted reflectance R_w, defined as,

$$R_w = \frac{\int_{\lambda_1}^{\lambda_2} R(\lambda) G_{AM1.5G}(\lambda) d\lambda}{\int_{\lambda_1}^{\lambda_2} G_{AM1.5G}(\lambda) d\lambda} \quad (1)$$

was calculated to evaluate its AR capability of the different structures. $R(\lambda)$ is the hemispherical reflectance (total optical reflectance) as a function of the wavelength and $G_{AM1.5}(\lambda)$ is the global spectral irradiance [31].

Optical transmission maps were obtained from the TCEs fabricated on glass by means of a home-made system combining a focused white-light lamp, an X-Y linear-positioner set, a pair of current preamplifiers, a reference photodiode and a pair of digital voltmeters (see Figure 3). The system is controlled by specific software that returns an image where each point registered is associated with a specific transmittance value. Once the data is collected, it is represented in the form of a histogram where two peaks appear: one of them corresponds to the background transmittance (T_B), and the other one is directly related to the combined transmittance of the sample plus the background (T_{SA}+T_B). T_{SA} comprises the transmittance of both the substrate and the different TCEs (TCO and/or GML). Thus, knowing the transmittance of the substrate (T_{SUB}), it is possible to calculate the amount of light transmitted by the different layers (T_{GG} for the GML and T_{TCO} for the TCO) as follows:

$$T_{GG+TCO+SUB} = \frac{T_{GG+TCO+SUB+B}}{T_B} \quad (2)$$

$$T_{GG+TCO} = \frac{T_{GG+TCO+SUB}}{T_{SUB}} \quad (3)$$

This measurement permits to verify the number of monolayers transferred and its effect on the transmittance of the whole TCE structure. In addition, the optical homogeneity of the TCE and the goodness of the graphene transferred can also be evaluated.

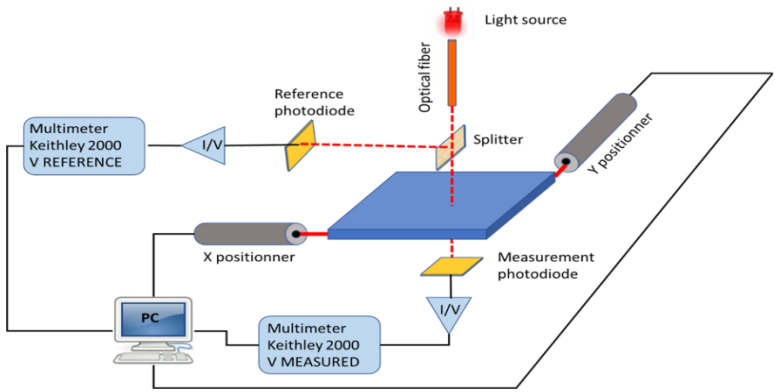

Figure 3: Scheme of the home-made system to determine the optical parameters in this work.

To determine the electrical parameters, four metal coplanar parallel electrodes of 0.1 cm width and 1 cm length unequally spaced (0.0366 cm, 0.0864 cm and 0.2379 cm, respectively), pictured in Figure 4, were deposited by thermal evaporation onto the samples. In the case of the GLM, they had been previously transferred onto 1 cm x 1 cm quartz substrates.

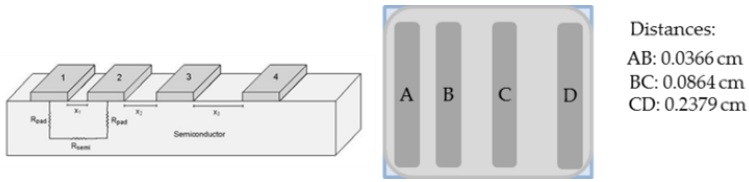

Figure 4: Schematic of the transmission line model (TLM) structure used to measure the electrical parameters of the fabricated TCEs.

The metal combination tested to have a low contact resistance was Ti (50nm)/Ag (500nm). Transmission-line-model (TLM) measurements [28] were done by testing 4-point electrical resistance. The electrodes were contacted by means of 4 micro-positioners, a power supply was used to bias the samples, an electrometer measured currents and a voltmeter provided voltages. The overall system is pictured in Figure 5.

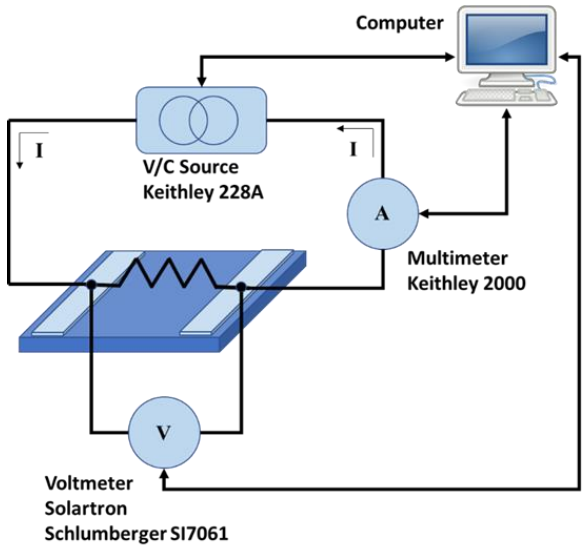

Figure 5: Scheme of the system used to determine the electrical parameters in this work.

These TLM measurements were used to determine the actual sheet resistance of the hybrid TCEs developed (R_{TCE}) and to compare them to the theoretical values expected corresponding to an electric circuit with two parallel electric resistances, as described by equation (4):

$$\frac{1}{R_{TCE}} = \frac{1}{R_{TCO}} + \frac{m}{R_{GG}} \quad (4)$$

where R_{TCO} is the sheet resistance of the TCO film, R_{GG}, the corresponding to 1 GML and m the number of GML.

A mapping of electrical conductance was carried out using non-contact and non-destructive commercial Onyx system from Das Nano Company, based on reflection-mode terahertz time-domain spectroscopy (THz-TDS) [29], where the measurable frequency range analyzed was from 0.1 THz to 5 THz. This patented system [30] provides a full-area map of conductance, resistance and other electrical parameters, related to 2D materials and thin films. The maps also show information about the homogeneity and quality of the deposition process. In addition, compared to other large-area methods, Onyx is capable to cover the gap between nano-scale and macro-scale methods. Its spatial resolution in the order of few hundreds of microns enables a fast characterization of large areas as opposed to microscopic methods.

Finally, the fabricated solar cells were characterized by measuring illuminated current-voltage characteristics at AM1.5G conditions and 100 mW/cm^2, using a class A solar simulator (Steuernagel SC575) and external quantum efficiency (EQE). Additionally, Suns-V_{oc} measurements were performed using the Sinton Instrument WCT-120 with the appropriate accessory stage to evaluate the series resistance (R_s) [32].

Results

In the following subsections, the quality of the graphene films as well as the evaluation of the compatibility of the preparation conditions, and the TCE optical and electrical performance are

presented. Lastly, results on solar cells where the top ITO has been replaced with the hybrid TCEs studies are also shown.

Graphene Quality

Raman spectra of the graphene films were used to evaluate the quality of the graphene films and transferring process. Three different spectra taken at random points in the substrates with 1, 2 and 3 graphene layers are displayed in Figure 6. All the spectra showed the characteristic peaks expected from graphene layers [33], mainly the G, G* and G' (or 2D as is also found in the literature) bands appearing at ~1590 cm^{-1}, ~2450 cm^{-1} and ~2690 cm^{-1} respectively. In Raman spectra of multilayered graphene stacks, the intensity ratio $I_{G'}/I_G$ was dependent on the number of graphene layers [27,33,34]. Experimentally, the intensity ratio exhibited a value $I_{G'}/I_G > 2$ for monolayers; $1 < I_{G'}/I_G < 2$ for bi-layers and $I_{G'}/I_G < 1$ for tri-layers and beyond. From the spectra shown in Figure 2, the intensity ratios for the samples with monolayers, bi-layers and tri-layers were 3.48, 1.00 and 0.82 respectively, which is consistent with the number of layers. This shows that the transferring process doesn't seem to widely introduce wrinkles or creases in the films otherwise the $I_{G'}/I_G$ intensity ratio would not agree with the number of layers transferred [23].

In addition to the G, G' and G* bands, a rather weak signal was also detected around 1350 cm^{-1} and 1620 cm^{-1}, corresponding to the D and D' bands. The presence of the D and D' bands require the existence of sp^3-C defects for its activation. In the spectra shown, the contribution of both peaks was very small and the defects were possibly rather localized since not all the spectra taken displayed these peaks. Nevertheless, some degree of imperfections seemed to be present in the transferred layers though probably not high enough as to have a negative effect in the proposed application.

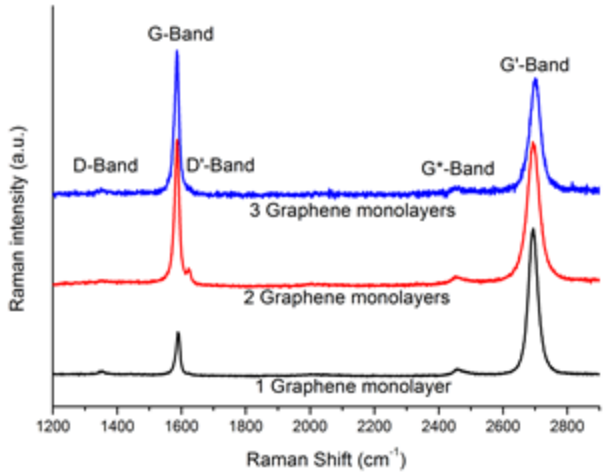

Figure 6: Raman spectra of the graphene layers transferred onto the ITO. The $I_{G'}/I_G$ ratio of the monolayer, bi-layer and tri-layer samples lies within the expected range, indicating a successful layer-by-layer transfer process.

Hybrid Graphene - TCO Transparent Contacts

Evaluation of the Compatibility of the Preparation Conditions

The compatibility between the conditions used in the graphene transfer method (chemical reagents, temperature in vacuum and in inert atmosphere, pressure or activation conditions in different environment, among others) and the temperature used to fabricate the solar cells was evaluated. It is very relevant to perform these analyses because the hybrid transparent contact based on graphene will be incorporated at the last manufacturing step. Hence, parameters such as the temperature and the environment used in the transfer process could negatively affect the performance of the material located underneath that constitutes the device. For this reason both, low- and high-temperature transfer procedures, were evaluated, while simultaneously avoiding O_2 plasmas and UV-O_3 gentle activation steps. The high temperature regime included processing steps at a temperature range from 200 to 450 ºC, that is, annealing in vacuum at 200 ºC, the use of temperature up 450 ºC in inert atmosphere, or both. Respectively, the low

temperature regime avoided those steps and the maximum temperature used was 120 ºC [14].

Table 1 shows the average white-light transmission, measured with the system pictured in Figure 3, and R_{GG}, measured with the system presented in Figure 5, for graphene samples varying the number of graphene monolayers transferred at high and low temperatures. For comparison, the electrical data given by the supplier, Graphenea S.L., are also included. In this case, the transfer was carried out using standard parameters on SiO_2/Si substrates [14].

Table 1: Average white-light transmission and sheet resistance R_{GG} for graphene samples with different number of monolayers transferred at respectively high and low temperatures. The nominal R_{GG} data of graphene materials transferred on SiO_2/Si provided by Graphenea (www.graphenea.com) [14] are included for comparison.

Number of graphene monolayers	Average white-light transmission (%)	R_{GG} (Ω/sq): transferred at high temperature regime on resistive glass	R_{GG} (Ω/sq): transferred at low temperature regime on resistive glass	Nominal R_{GG} (Ω/sq): transferred at standard conditions on SiO_2/Si
1	97.6± 1.0	375 ± 25	295 ± 25	350 ± 50
2	95.7± 1.0	175 ± 10	155 ± 10	188 ± 3
3	93.3± 0.9	120 ± 15	125 ± 15	126 ± 6

It can be noticed that the average white-light transmission values were in agreement with the theoretical predictions made according to the number of graphene monolayers [35]. Therefore, that parameter was not affected by the temperature used during the transfer process. In the case of R_{GG}, a slight electrical improvement was observed in the graphene material transferred at low temperature. This result demonstrates that the temperature of the graphene transferring process can be reduced without altering the material performance. Furthermore, the low substrate temperature would also benefit the deposition of the hybrid transparent contacts based on a TCO by reducing the possible damage to it.

In a second step, the position of graphene monolayer within the hybrid transparent contact structure, i.e. below the TCO or on the TCO, was evaluated. This way, the possible damage to graphene material produced by the bombardment of the high-energy sputtered particles during the TCO deposition would be highlighted. For that, three graphene monolayers were transferred at low temperature onto: (i) a TCO-coated resistive glass (structure 1, in Table 2) and (ii) a bare quartz substrate, which would be subsequently covered with a TCO (structure 2, in Table 2). In both structures, the TCO used was a 40-nm thick sputtered ITO thin film. Table 2 shows the optoelectronic properties obtained for both structures under study.

Table 2: Sheet resistance R_{sheet} (R_{TCE}, R_{TCO} or R_{GG}) and average white-light transmission for the structures under study where the graphene trilayer is located in different positions. The optoelectronic data of the ITO thin film and the graphene trilayer transferred onto quartz are included for comparison.

	R_{sheet} (Ω/sq)	Average white-light transmission (%)
ITO (40 nm)/Glass	196.5 ± 1.0	89 ± 5
3 Graphene monolayers/Quartz	120.0 ± 5.0	93 ± 2
Structure 1: 3 Graphene monolayers/ITO (40 nm)/Glass	156.5 ± 15.0	80 ± 6
Structure 2: ITO (40 nm)/3 graphene monolayers/Quartz	200.0 ± 34.0	78 ± 4

These data revealed that better optoelectronic properties are obtained for the structure 1, in which the graphene was transferred onto the ITO coated glass. These results confirm the potential damage on graphene caused by the sputtering deposition, leading to a worsening of the transparent-contact performance [36].

Role of the TCO on the Hybrid Transparent Contacts

Taking the results described above into account, the hybrid transparent contacts were fabricated based on configuration 1 shown in Figure 1a) (the graphene transferred on top of a TCO-

coated substrate) and using a low temperature transfer method for the graphene layers. Both, AZO and ITO materials were incorporated into the contact to assess the effect of the TCO in the optical and electrical performance of the contact. From the optical point of view, the main role of the TCO is to act as an AR coating, diminishing the amount of light reflected on the solar-cell surface; that means, to eliminate unwanted reflection and increase the overall transparency. Hence, the thickness of the TCO must be fitted so that the wavelength in the material is one quarter the wavelength of the incoming wave, according to the formula (5)

$$nd = \frac{\lambda}{4}, \tag{5}$$

where n is its refractive index, d is its thickness and λ is the wavelength. For photovoltaic applications, thickness is chosen in order to minimize reflection for a wavelength of 0.6 μm. This wavelength is chosen because it is close to the peak power of the solar spectrum [21]. Therefore, the thickness of AZO and ITO was close to 80 nm.

From the electrical point of view, the TCO must present the lowest possible resistivity to reduce device resistance and to extract the current in the most efficient way. Under these considerations, the performance of the hybrid transparent contacts was evaluated from the figure of merit (FOM) ϕ proposed by Haacke [37] given by the following formula (6):

$$\phi\,(\Omega^{-1}) = T^{10}/R_{TCE}\,(\Omega/sq), \tag{6}$$

where T^{10} is the average optical transmittance.

Table 3 summarizes the optoelectronic results achieved by the different hybrid transparent contacts fabricated in this work, where either one two or three graphene monolayers were combined with ITO or AZO. It can be noticed that R_{TCE} clearly depends on the TCO material used: A detriment was obtained when AZO was used. This may be attributed to a possible diffusion of the Al atoms from AZO occurring in the whole structure, which would negatively affect the electrical

performance of the graphene monolayer located at the graphene/AZO interface [17,38,39]. For this reason, R_{TCE} obtained with three graphene monolayers transferred on top saw a clear improvement, compared to the one that incorporated two monolayers. In any case, R_{TCE} of the AZO-based hybrid transparent contact was not much lower than the R_{TCO} of the bare 80 nm-thick AZO layer of 120 ± 10 Ω/sq.

Table 3: R_{TCE}, average white-light transmission and figure of merit calculated for the hybrid transparent contacts in study depending on the TCO material and the number of the graphene monolayers transferred.

Nº graphene monolayers	80 nm-thick TCO material	R_{TCE} (Ω/sq)	Average white-light transmission (%)	FOM (x 10^{-4} Ω^{-1})
2	AZO	890 ± 70	86 ± 2	2.4 ± 0.9
3	AZO	116 ± 6	80 ± 3	9.2 ± 0.5
1	ITO	85 ± 5	85 ± 2	23.2 ± 0.4

On the other hand, a different electrical behavior was achieved when ITO was incorporated into the hybrid transparent contact. No deterioration was observed in R_{TCE} in comparison with the R_{TCO} of bare 80 nm-thick ITO layer of 85 ± 5 Ω/sq. Hence, it may be assumed that no damage would take place at the graphene/ITO interface. Finally, the best FOM value was achieved when ITO was incorporated into the hybrid transparent contact, even while incorporating only one graphene monolayer. Hence, the hybrid contact based on ITO and one monolayer presented the best optoelectronic performance.

Optical Performance of the Hybrid Transparent Contacts

The addition of graphene monolayers onto the ITO surface necessarily modifies the optical characteristics of the transparent conductive electrode. The most straightforward effect is the loss in optical transmittance, which has been found to be about 3% in average with each additional graphene sheet in the wavelength of interest for SHJ solar cells [40,41]. In the case of SHJ solar cells, not only the transmittance is relevant, is also important to evaluate the reflectivity of the structure since the TCE also

serves the role of an AR coating. The reflectance spectra of the TCEs deposited onto crystalline silicon can be seen in Figure 7.

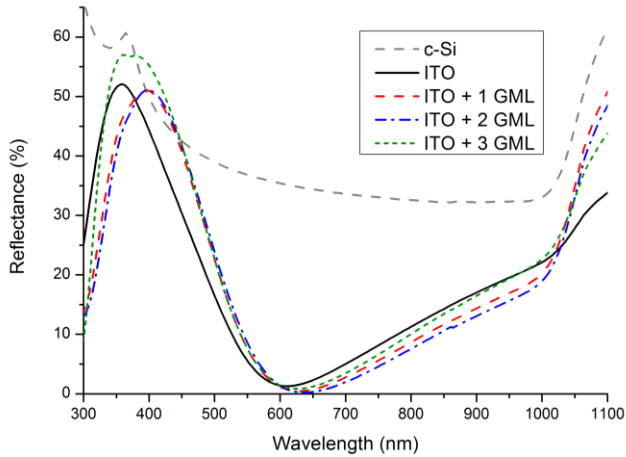

Figure 7: Reflectance spectra measured for the cells with only ITO as the TCE and the cells with a hybrid TCE consisting in a layer of ITO and either one, two or three graphene monolayers. The reflectance spectra of a bare polished silicon wafer is also shown for reference.

The spectra obtained were typical for an AR coating deposited on a polished silicon wafer. As can be seen, the presence of ITO is able to greatly reduce the reflectivity of the Si polished wafer (also shown in Figure 7 for reference), especially between 400 nm and 1000 nm. Focusing on the effect of adding 1 or 2 graphene monolayers onto the ITO, we can observe how the minimum in reflectance shifts towards slightly longer wavelengths. This shift can be understood by reviewing the refractive indexes of the films involved. The thickness of the ITO films were chosen so that the minimum in reflectance occurs at a wavelength $\lambda \approx 600$ nm according to the condition described in formula (5) [42]. By adding the graphene layers, since the refractive index of graphene in that wavelength range is reported to be around $n \approx 2.5$ [43] i.e. above that of ITO ($n \approx 2$), λ had to shift towards higher wavelengths since the thickness remains practically unchanged. In the case of 3 graphene monolayers, the reflectance spectra measured deviated from the trend created with 1 and 2 monolayers and the minimum shifts again towards lower wavelengths. Besides the shift in the

position of the minimum, it is also relevant to assess the AR properties of the TCEs. To do so, the average reflectance weighted by the AM1.5G spectrum can be calculated in the wavelength range of interest according to formula 1.

From Figure 7, it is clear that the hybrid TCEs provide better AR properties if the wavelength range is limited to 600 - 1050 nm, whereas outside that range, ITO mostly has a better performance. However, the majority of the response of the solar cells studied in this research occurs in a much narrower range than that shown in Figure 7. For example, around 95% of the J_{sc} of the solar cells is generated in the wavelength range between 430-1050 nm as calculated by integrating their external quantum efficiencies (not shown). In that range, the differences in R_w for the 4 structures studied are very small. If the range is narrowed even further to 600-1050 nm, the contribution to J_{sc} represent around 80% of the total and, in that range, the hybrid TCEs show up to a 2.8% lower R_w. For clarity, Table 4 gathers the values of R_w in those particular wavelengths.

Table 4: Weighted reflectance calculated from the spectra shown in Figure 8 in two different wavelength ranges. The range between 430-1050 nm is relevant because it represents around 95% of the photogenerated current; the range between 600-1050 nm is the range where the hybrid TCE is clearly better in terms of antireflectance properties and it accounts for around 80% of the photogenerated current.

TCE	R_w 430-1050 nm (~95% J_{sc})	R_w 600-1050 nm (~80% J_{sc})
ITO	12.05%	10.51%
ITO + 1 GML	12.76%	8.65%
ITO + 2 GML	12.56%	7.74%
ITO + 3 GML	13.62%	9.81%

Electrical Performance of the Hybrid Transparent Contacts

The main interest in introducing graphene into the solar cell structure is to improve the electrical properties of the transparent conductive electrode (while sacrificing as little as possible of the optical characteristics). In order to characterize the sheet resistance in situ, a contactless technique such as THz-TDS is highly convenient. In Figure 8 are shown the maps of the

conductance obtained with ITO (a) and with ITO + 1(b), +2(c) and +3(d) graphene monolayers. Undoubtedly, the colormaps showed a clear improvement in the TCE conductance as more graphene layers are added.

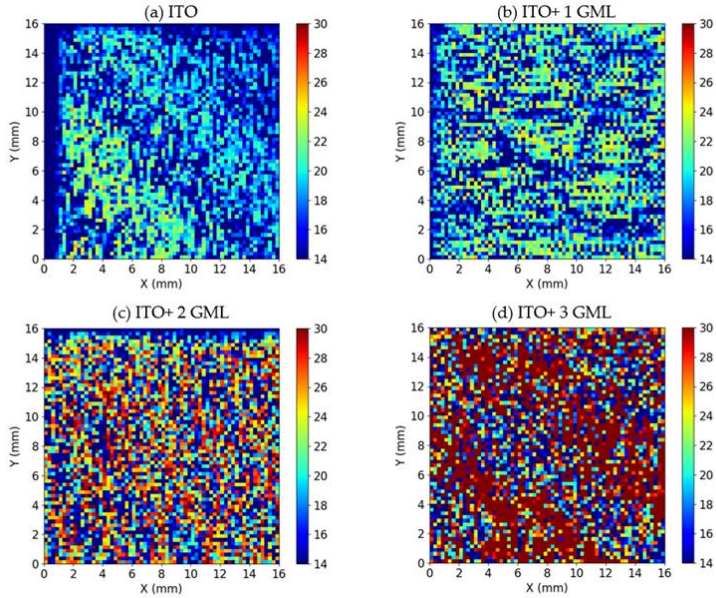

Figure 8: Reflection-mode terahertz time-domain spectroscopy results obtained with bare ITO (a) and with ITO + 1(b), +2(c) and +3(d) graphene monolayers as the front contact TCE.

When translated into sheet resistance, the conductance maps yielded average values that decreased from 60.2 Ω/sq for the cell with bare ITO, to 54.9 Ω/sq, 47.2 Ω/sq and 37.7 Ω/sq for the cells with 1, 2, and 3 graphene monolayers respectively. Previous results obtained using transmission line measurements [41] revealed a sheet resistance for the ITO of 59 Ω/sq while the graphene layers have a sheet resistance of 450 ± 50 Ω/sq [14]. Since the sheet resistance sees the ITO film and the graphene layers as connected in parallel [44], the obtained values should decrease according to equation (4). The values obtained using THz-TDS and the range of expected values considering R_{TCO}=60.2 Ω/sq and R_{GG}=450 ± 50 Ω/sq are plotted in Figure 9. As can be observed, the values obtained match very well the anticipated values. Therefore, the results indicate there is a good

electrical contact between all layers and the hybrid TCE should outperform bare ITO in terms of the lateral collection of carriers that reaches the TCE.

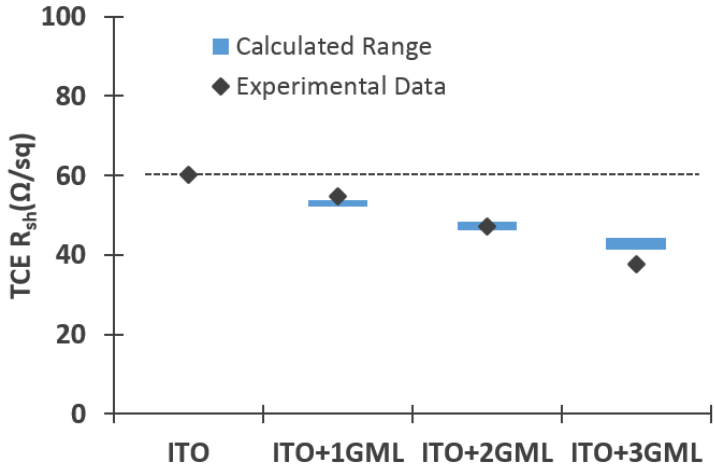

Figure 9: Measured sheet resistance (scatter plot) using THz-TDS and the calculated range of values (blue colored areas) according to equation (7), considering a sheet resistance for the graphene monolayers of 450 ± 50 Ω/sq. The dotted line is a guide to the line positioned at a value equal to the measured ITO sheet resistance.

Solar Cells Performance

On the basis of previous results shown, in this section we focused on evaluating the effect of going beyond one graphene monolayer. In Figure 10, the changes in J_{sc}, V_{oc}, FF, R_s and the overall efficiency η of the cells with hybrid TCEs, with respect to the reference cell with only ITO are presented. Starting with the values of V_{oc} in Figure 10a, the soft techniques used for transferring the sheets (thus not damaging the underlying layers) and the fact that the sheets are far from the junction means they should not alter the values. Indeed, we found the V_{oc} measured in the cell with only ITO (708 mV) remained practically unchanged in the cells with a hybrid TCE (707 mV). The values of J_{sc} on the other hand saw a strong decrease when more than one graphene monolayer was used. Again, with the addition of a single graphene layer, the loss in transmittance is mostly offset by the improvement in reflectance in a large part of the usable light and

only a 1% in J_{sc} is lost. But with the addition of a second and third monolayer the loss in transmittance clearly dominates the optical response and the loss in J_{sc} worsens to 5.5% and 10.5% respectively.

Figure 10b recapitulates the changes in FF and R_s. As shown, the improvements in these cases are noticeable. As the top contact ITO was replaced with an hybrid TCO with one, two or three graphene monolayers, the value of R_s decreased from 2.46 $\Omega \cdot cm^2$ down to 2.10 $\Omega \cdot cm^2$, 1.83 $\Omega \cdot cm^2$ and 1.65 $\Omega \cdot cm^2$ respectively; likewise, the FF increased from 70.7% to 72.6%, 73.5% and 74.6% accordingly. The observed trend is in line with the improvements in sheet resistance of the TCEs obtained with each additional graphene monolayer shown in Figure 9. In additional, a better work function matching between the Ti electrode and the ITO, and thus a lower junction barrier, is also expected thanks to the presence of graphene. The work function of Ti is 4.33 eV whereas in ITO is close to 5.0 eV. According to [23,45], the work function of graphene multilayer stacks depends on the number of monolayers, increasing from 4.32 eV for one monolayer, up to 4.55 eV in the case of a three monolayer stack. Hence, the barrier between Ti and ITO is reduced with each graphene monolayer which would also help in improving the series resistance of the devices [25].

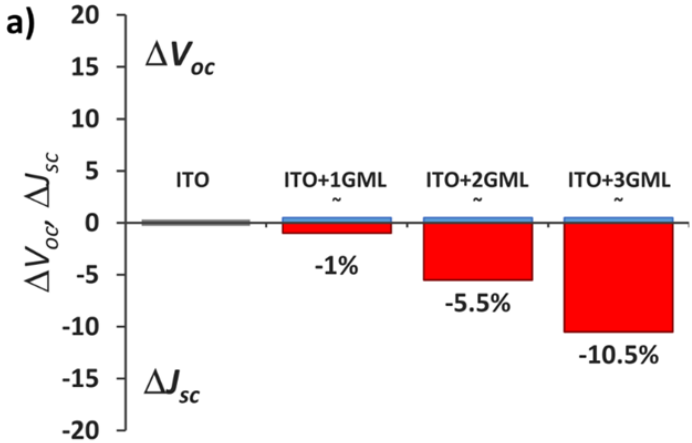

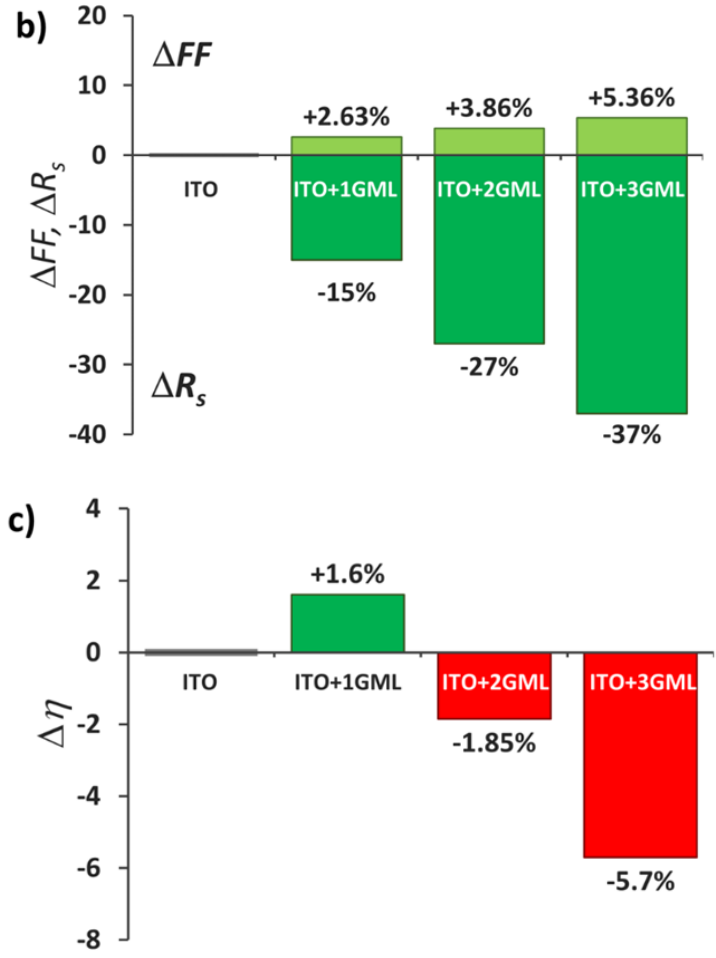

Figure 10: Solar cell parameters variations (V_{oc} and J_{sc} (a), FF and R_s (b) and overall efficiency η (c)) observed as the front ITO is substituted by a hybrid TCE consisting in an ITO layer covered with one, two or three graphene monolayers.

Lastly, the effect to the overall efficiency is summarized in Figure 10c. Since the value of V_{oc} remained practically unchanged, the effect of the added graphene monolayers on the efficiency is the result of the compromise between the improved electrical characteristics and the worsening of the optical transparency of the TCE. As a result, the device with a single graphene monolayer displayed a 1.6% higher efficiency

compared to the reference cell, but the cells with two and three monolayers suffered an efficiency drop of 1.85% and 5.7% respectively. The results obtained with the finished solar cells also agrees with the FOM for the hybrid electrodes calculated in Section 3.2.2 where the structure fabricated with ITO and 1 GML showed the best performance for a TCE.

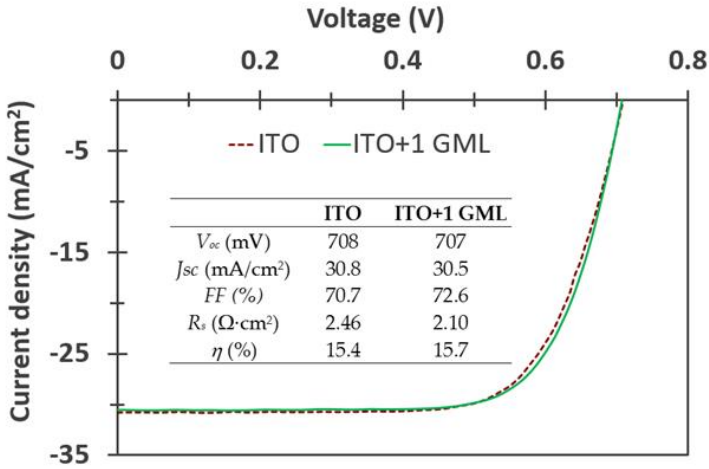

Figure 11: JV characteristics under illumination of the cells with either ITO as the front TCE and with the ITO layer covered with one graphene monolayer.

To conclude, in Figure 11 the current-voltage characteristics under AM1.5G illumination and the extracted parameters for the cells with ITO and with ITO + 1 GML are shown. These results demonstrate that there is potential in hybrid TCEs based on graphene and transparent conductive oxides. The addition of the graphene monolayers to the ITO clearly improve its electrical characteristics and the improvements are transferred to the JV characteristics of the solar cells, which display a better R_s and FF. The loss in transmission caused with each graphene monolayer means that they need to be kept at a minimum, otherwise the drop in J_{sc} can be significant. However, in addition to what we have shown there is still clear room for improvement. Among other things, the electrical conductivity of graphene can be increased via chemical doping without sacrificing its transparency [46]; and the thickness of the TCO can be further optimized for hybrid structures as deduced from the reflectance

spectra shown in Figure 7. All these prospects invites to further study hybrid electrodes based on graphene as a promising alternative for next generation solar cells and compatible upcoming technologies.

Conclusions

This work presents the evaluation of the preparation protocols used in the fabrication of hybrid transparent contacts based on a common TCO and graphene monolayers. The first parameter evaluated was the temperature used during the graphene transfer process. Reduced sheet-resistance values of the graphene monolayers were obtained at low temperature. The optimum spatial configuration of the layers forming the hybrid transparent contacts was also determined. A strong effect on the electrical properties of graphene due to the bombardment of the highly-energetic sputtered atoms during the sputtering process of the TCO thin film was observed. Hence, adequate preparation conditions should include transferring the graphene monolayers onto the TCO and not the opposite. A correlation between the avoidance of aluminum (both in the metal contact and in the TCO) and good and repeatable electrical properties were found. Combinations of graphene with ITO were systematically better than those of graphene and AZO. Therefore, the combination of ITO and Graphene in a hybrid transparent contact was found to have an appropriate performance to be used as an electrode in optoelectronic devices.

This work also presents a study on hybrid transparent conductive electrodes based on ITO and graphene and its application as front contacts in silicon heterojunction solar cells. The electrodes consisted of up to three monolayers of CVD-synthesized graphene transferred onto the top of ITO in silicon heterojunction solar cells. The effect of the graphene layers on the reflectance spectra depended on the wavelength range considered. In the range between 430–1050 nm (which corresponds to around 95% of the generated photocurrent) a small increase in the weighted reflectance not larger than 1.5% was observed. In the range between 600–1050 nm (which corresponds to around 80% of the generated photocurrent) all of

the cells with graphene on top showed better AR properties than the reference cell. The electrical characterization through THz time domain spectroscopy illustrated good electrical contact between the ITO and the stacks of graphene monolayers. For all cases, the sheet resistance of the ITO layer was reduced accordingly to an intimate parallel combination of all the layers. The current–voltage characteristics of the solar cells with graphene showed a better series resistance and FF thanks to the improved sheet resistance and work function matching between the transparent electrode and the metal grid, while the cells' V_{oc} was hardly affected. On the other hand, J_{sc} decreased with each graphene monolayer due to a lower optical transmission of the electrode. This effect was mostly cancelled out for one graphene monolayer by the improvement in reflectance in a large part of the usable light, and only 1% of J_{sc} was lost. Overall, the cell with a single graphene monolayer displayed a 1.6% higher efficiency compared to the reference cell, while the cells with two and three monolayers could not improve upon that. These results show that graphene can be used to improve the conductance of ITO and that its application can be helpful in increasing the efficiency of solar cells. Furthermore, new strategies to improve the chemical doping of graphene monolayers without sacrificing its transparency are being studied worldwide. The application of such strategies to hybrid electrodes based on graphene, or even to electrodes based on multilayered graphene alone, opens up the possibility of fabricating high-performance electrodes suitable for use in next-generation solar cells and upcoming technologies.

All these approaches have an enormous potential to open new horizons to achieve the definitive take-off graphene technologies for electrical standard and transparent contacts.

References

1. Geim AK, Graphene Prehistory. Phys. Scr. 2012; T146: 0140034.
2. Ruess G, Vogt F. Höchstlamellarer Kohlenstoff aus Graphitoxyhydroxyd. Monatshefte für Chemie. 1948; 78: 222–242.

3. Novoselov KS, Geim AK, Morozov SV, Jiang D, Zhang Y, et al. Electric Field Effect in Atomically Thin Carbon Films. Science. 2004; 306: 666–669.
4. Kusmartsev FV, Wu WM, Pierpoint MP, Yung KC. Application of Graphene within Optoelectronic Devices and Transistors. 2014; arXiv: 1406.0809, 1-17.
5. Bonaccorso F, Sun Z, Hasan T, Ferrari AC. Graphene photonics and optoelectronics. Nature Photon. 2010; 4: 611–622.
6. Saive R, Borsuk AM, Emmer HS, Bukowsky CR, Lloyd JV, et al. Effectively Transparent Front Contacts for Optoelectronic Devices. Adv. Optical Mater. 2016; 4: 1470–147.
7. Tonny KN, Rafique R, Sharmin A, Bashar MS, Mahmood ZH. Electrical, optical and structural properties of transparent conducting Al doped ZnO (AZO) deposited by sol-gel spin coating. AIP Advances. 2018; 8: 065307 (7pp).
8. Zinchenko TO, Pecherskaya EA, Nikolaev KO, Golubkov PE, Shepeleva YV, et al. The study of the optical properties of transparent conductive oxides SnO2:Sb, obtained by spray pyrolysis. J. PhyS. Conf. Ser. 2019; 1410: 012090 (5pp).
9. Meza D, Cruz A, Morales-Vilches AB, Korte L, Stannowski B. Aluminum-Doped Zinc Oxide as Front Electrode for Rear Emitter Silicon Heterojunction Solar Cells with High Efficiency. Appl. Sci. 2019; 9: 862 (10pp).
10. Giubileo F, Di Bartolomeo A. The role of contact resistance in graphene field-effect devices. Prog. Surf. Sci. 2017; 92: 143-175.
11. Yue DW, Ra CH, Liu XC, Lee DY, Yoo WJ. Edge contacts of graphene formed by using a controlled plasma treatment. Nanoscale. 2015; 7: 825–831.
12. Gahoi A, Wagner S, Bablich A, Kataria S, Passi V, et al. Contact resistance study of various metal electrodes with CVD graphene. Solid-State Electron. 2016; 125: 234–239.
13. H Zhong, Z Zhang, B Chen, H Xu, D Yu, et al. Realization of low contact resistance close to theoretical limit in graphene transistors. Nano Research. 2015; 8: 1669– 1679.
14. Available Online at: https://www.graphenea.com/pages/cvd-graphene#.XpwPesgzbIV.

15. Nagashio K, Nishimura T, Kita K, Toriumi A. Contact resistivity and current flow path at metal/graphene contact. Appl. Phys. Lett. 2010; 97: 143514 (3pp).
16. Robinson JA, LaBella M, Zhu M, Hollander M, Kasarda R, et al. Contacting graphene. Appl. Phys. Lett. 2011; 98: 053103 (3pp).
17. Rashad M, Pan F, Yu Z, Asif M, Lin H, et al. Investigation on microstructural, mechanical and electrochemical properties of aluminum composites reinforced with graphene nanoplatelets. Prog. Nat. Sci. Mater. 2015; 25: 460–470.
18. Moon JS, Antcliffe M, Seo HC, Curtis D, Lin S, et al. Ultra-low resistance ohmic contacts in graphene field effect transistors. Appl. Phys. Lett. 2012; 100: 203512 (3pp).
19. Zhu SE, Yuan S, Janssen GCAM. Optical transmittance of multilayer graphene. EPL. 2014; 108: 17007 (4 pages).
20. Yamamoto K, Yoshikawa K, Uzu H, Adachi D. High-efficiency heterojunction crystalline Si solar cells. Jpn. J. Appl. Phys. 2018; 57: 08RB20.
21. Wang EC, Morales-Vilches AB, Neubert S, Cruz A, Schlatmann R, et al. In A simple method with analytical model to extract heterojunction solar cell series resistance components and to extract the A-Si:H(i/p) to transparent conductive oxide contact resistivity, Silicon PV 2019, the 9th International Conference on Crystalline Silicon Photovoltaics. 2019; 6.
22. Hecht DS, Hu L, Irvin G. Emerging transparent electrodes based on thin films of carbon nanotubes, graphene, and metallic nanostructures. Advanced Materials. 2011; 23: 1482-1513.
23. Lancellotti L, Bobeico E, Della Noce M, Mercaldo LV, Usatii I, et al. Graphene as non-conventional transparent conductive electrode in silicon heterojunction solar cells. Appl. Surf. Sci. 2020; 525: 146443.
24. Liu J, Yi Y, Zhou Y, Cai H. Highly Stretchable and Flexible Graphene/ITO Hybrid transparent electrode. Nanoscale Research Letters. 2016; 11: 7.
25. Fernandez S, Molinero A, Sanz D, Gonzalez JP, Cruz M, et al. Graphene-Based Contacts for Optoelectronic Devices. Micromachines (Basel). 2020; 11.

26. Demaurex B, De Wolf S, Descoeudres A, Charles Holman Z, Ballif C. Damage at hydrogenated amorphous/crystalline silicon interfaces by indium tin oxide overlayer sputtering. Appl. Phys. Lett. 2012; 101: 171604.
27. Hao Y, Wang Y, Wang L, Ni Z, Wang Z, et al. T, Probing layer number and stacking order of few-layer graphene by Raman spectroscopy. Small. 2010; 6: 195-200.
28. Nagashio K, Nishimura T, Kita K, Toriumi A. Contact resistivity and current flow path at metal/graphene contact. Appl. Phys. Lett. 2010; 97: 143514 (3pp).
29. Bøggild P, Mackenzie DMA, Whelan PR, Petersen DH, Buron JD, et al. Mapping the electrical properties of large-area graphene. 2D Materials. 2017; 4: 042003.
30. Azanza E, Chudzik M, López A, Etayo D, Hueso LE, et al. Das Nano, S.L. Quality inspection of Thin films materials. Unites States patent, US 10,267,836 (B2). 2019 April 23.
31. Gagliano A, Nocera F, Patania F, Contino A. A procedure for the characterization of the solar-weighted reflectance of mirrored reflectors. In Proceedings of the 2014 5th International Renewable Energy Congress (IREC). Hammamet, Tunisia. 2014.
32. Pysch D, Mette A, Glunz SW. A review and comparison of different methods to determine the series resistance of solar cells. Sol. Energy Mater. Sol. Cells. 2007; 91: 1698–1706.
33. Malard LM, Pimenta MA, Dresselhaus G, Dresselhaus MS. Raman spectroscopy in graphene. Phys. Rep. 2009; 473: 51-87.
34. Nguyen VT, Le HD, Nguyen VC, Tam Ngo TT, Le DQ, et al. Synthesis of multi-layer graphene films on copper tape by atmospheric pressure chemical vapor deposition method. Adv. Nat. Sci.: Nanosci. Nanotechnol. 2013; 4: 035012.
35. Zhu SE, Yuan S, Janssen GCAM. Optical transmittance of multilayer graphene. EPL Europhys. Lett. 2014; 108: 17007.
36. Ahlberg P, Johansson FOL, Zhang ZB, Jansson U, Zhang SL, et al. Defect formation in graphene during low energy ion bombardment. APL Mater. 2016; 4: 046104.
37. Haacke G. New figure of merit for transparent conductors. J. Appl. Phys. 1976; 47: 4086.
38. Abushanab WS, Moustafa EB, Ghandourah E, Taha MA. Effect of graphene nanoparticles on the physical and

mechanical properties of the Al2024-graphene nanocomposites fabricated by powder metallurgy. Results Phys. 2020; 19: 103343.
39. Yolshina LA, Muradymov RV, Vichuzhanin DI, Smirnova EO. Enhancement of the Mechanical Properties of Aluminum Graphene Composites. AIP Conf. Proc. 2016; 1785: 040093.
40. Zhu SE, Yuan S, Janssen GCAM. Optical transmittance of multilayer graphene. EPL. 2014; 108: 17007.
41. Torres I, Fernández S, Gandía JJ, González N, Barrio R, et al. In Graphene-based transparent electrode incorporated into silicon heterojunction solar cell technology, 37th European Photovoltaic Solar Energy Conference and Exhibition. 2020; 478-481.
42. van Sark WGJHM, Korte L, Roca F. (Eds.) Physics and Technology of Amorphous-Crystalline Heterostructure Silicon Solar Cells. Berlin: Springer. 2012
43. Ochoa-Martinez E, Gabas M, Barrutia L, Pesquera A, Centeno A, et al. Determination of a refractive index and an extinction coefficient of standard production of CVD-graphene. Nanoscale. 2015; 7: 1491–1500.
44. Fernández S, Bosca A, Pedros J, Ines A, Fernández M, et al. Advanced Graphene-Based Transparent Conductive Electrodes for Photovoltaic Applications. Micromachines. 2019; 10: 402.
45. Lancellotti L, Polichetti T, Ricciardella F, Tari O, Gnanapragasam S, et al. Graphene applications in Schottky barrier solar cells. Thin Solid Film. 2012; 522: 390–394.
46. Bianco GV, Sacchetti A, Milella A, Grande M, D'Orazio A, et al. Extraordinary low sheet resistance of CVD graphene by thionyl chloride chemical doping. Carbon. 2020; 170: 75–84.